Cyclic behavior of hollow-core diaphragm subassemblies

Nelson M. Angel, Juan F. Correal, and José I. Restrepo

- An experimental program was performed to study the effect of seismic loading on precast concrete diaphragms consisting of hollow-core slabs and subjected to various loading and boundary conditions.
- Precast concrete diaphragm specimens were developed consisting of either two or three hollow-core slabs and were loaded either parallel or orthogonally to the longitudinal joints. Four specimens were developed for the program, of which three were untopped and one included a cast-in-place concrete topping.
- The specimens were tested with reverse cyclic loading, and the test results provided comparison data related to the influence of various parameters, such as the bidirectional loading conditions and the performance of the cast-in-place concrete topping for the fourth specimen.

PCI Journal (ISSN 0887-9672) V. 64, No. 2, March–April 2019.

PCI Journal is published bimonthly by the Precast/Prestressed Concrete Institute, 200 W. Adams St., Suite 2100, Chicago, IL 60606.

The 1994 Northridge earthquake in California highlighted the importance of diaphragm behavior for the overall response of precast concrete buildings. The damage observed in precast concrete diaphragms and the collapse of several buildings during this earthquake motivated the industry to understand and resolve the causes of undesirable seismic performance.[1] Immediately following the event, in response to the performance of precast concrete diaphragms, several requirements were introduced in codes and specifications, such as the American Concrete Institute's (ACI's) *Building Code Requirements for Structural Concrete (ACI 318-99) and Commentary (ACI 318R-99)*,[2] the *Uniform Building Code*,[3] and the National Earthquake Hazards Reduction Program's (NEHRP's) *Recommended Provisions for Seismic Regulations for New Buildings and Other Structures*.[4,5] Some of these provisions were intended to ensure some ductility capacity in diaphragm elements.

Seismic design procedures for precast concrete diaphragms have been recently reexamined. The comprehensive methodology developed by the DSDM (Diaphragm Seismic Design Methodology) Consortium[6–8] was adopted into the American Society of Civil Engineers' ASCE 7-16[9] and the 2015 NEHRP provisions.[10] However, the use of untopped precast concrete diaphragms in high seismic regions remains largely unexplored and lacks experimental evidence. In a paper on proposed revisions to the 1997 NEHRP provisions, Hawkins and Ghosh[11] suggest that if elastic behavior is ensured for untopped precast concrete diaphragms under design seismic demands, then there are no fundamental differences or advantages in incorporating a cast-in-place concrete topping slab on precast concrete units. The authors proposed untopped

hollow-core diaphragms to be designed for in-plane forces large enough to ensure elastic behavior under high-intensity earthquakes and to provide ductility to ensure some redistribution of the internal forces in the diaphragm. Furthermore, early results on the experimental behavior of hollow-core slabs incorporating waved joints proposed by Menegotto and Monti[12] indicated that they could be a successful alternative to reduce the perceived deficiencies of untopped hollow-core diaphragms in high seismic zones. Cleland and Ghosh[5] described how untopped precast concrete diaphragms might be designed for building structures in high seismic zones complying with ACI 318-14[13] requirements. The authors suggested that when using untopped diaphragms, it is necessary to demonstrate that the system satisfies the equivalency requirement set forth in ACI 318 as follows: "A reinforced concrete structural system not satisfying this chapter shall be permitted if it is demonstrated by experimental evidence and analysis that the proposed system will have strength and toughness equal to or exceeding those provided by a comparable reinforced concrete structure satisfying this chapter." In their work, the authors outlined how the equivalency requirement could be achieved and highlighted the need for further research.

The use of untopped hollow-core slabs as diaphragms in seismic regions may be a practical and economical construction alternative if the perimeter reinforcement and connection details are appropriately designed with optimum use of materials, slenderness of construction, environmental friendliness, and reduced self-weight of the floors (**Fig. 1**). A reduction in floor inertia forces due to earthquake actions could be also expected.

This paper summarizes the results of an experimental program of a comprehensive research project on hollow-core diaphragms with a low aspect ratio in buildings where all of the vertical elements (walls and columns) are part of the lateral-force-resisting system and are tied by beams of moment-resisting frames. The primary objective of the experimental research was to study the cyclic performance of hollow-core diaphragm subassemblies where the hollow-core slabs are confined by beams of moment-resisting frames. Three large-scale, untopped hollow-core diaphragm specimens were tested under reversed cyclic loading using a bidirectional test fixture for simultaneous control of in-plane lateral load and bending deformations. A fourth specimen, which uses a cast-in-place concrete topping slab in composite action with hollow-core slabs, was also tested for comparison purposes. Detailed analysis of the test results and observations are presented.

Figure 1. Construction of an untopped hollow-core diaphragm incorporating connection details in broken cores. Photo courtesy of Manufacturas de Cemento SA.

Experimental investigation

The cyclic behavior of four large-scale specimens resembling a hollow-core subdiaphragm region framed by beams was studied experimentally. Three specimens were constructed as untopped hollow-core diaphragms with variations in the orientation and number of hollow-core units. The variation in the orientation of the hollow-core slabs within the specimen with respect to the cyclic demand enabled the study of two boundary conditions: an upper-bound condition with very high in-plane stiffness and high strength of the framing beams and a more flexible boundary condition to evaluate the influence of the in-plane flexural stiffness and flexure strength of the framing beams. Increased flexibility of the boundary conditions was also studied with the addition of a third hollow-core slab. These boundary conditions could be representative of actual subdiaphragm regions. A fourth specimen was constructed, and it incorporated a 50 mm (2 in.) thick cast-in-place concrete topping slab according to the requirements for composite action.[13] The specimens were tested under a quasi-static reversed cyclic loading protocol of groups of three symmetric shear distortion γ cycles at increasing amplitudes. After the application of each level of shear distortion, the specimens were inspected to assess the progressive damage. The test specimens were built, instrumented, and tested at the Alberto Sarria Laboratory of Structural Models at Universidad de los Andes in Bogotá, Colombia.

Specimens details and test setup

Table 1 provides the cross-sectional properties of the hollow-core units used in this study. A span-to-depth ratio of 30 for the hollow-core units was selected to control excessive floor vibrations that might affect the serviceability of hollow-core floors. **Figure 2** shows diagrams of the test specimens. The convention for identifying the specimens was two letters followed by a number in the following order: U and T for untopped and topped specimens, respectively; P and O for cyclic demand applied parallel or orthogonally (perpendicular) to the longitudinal joints, respectively; and a number indicating the quantity of hollow-core slab units used in the specimen. Two types of untopped specimens were tested for each of the boundary conditions provided by the orientation of the hollow-core slabs. Specimen UO2 (Fig. 2, with the hollow-core slabs running perpendicularly to the direction of the in-plane demands, represented the upper-bound condition due to the high in-plane stiffness and strength provided by the test beams located at the fixed and movable ends, also affecting the kinematics of the hollow-core slabs. In-plane bend-

Table 1. Cross-sectional properties of the hollow-core units

Width, mm	Thickness, mm	Core diameter, mm	Cores' center-to-center spacing, mm	Number of cores	Top and bottom flange depth, mm	Web width, mm	Cross-section area, mm²
1195	100	58	75.6	15	21	17.6	76,469

Note: 1 mm = 0.0394 in. 1 mm² = 0.00155 in.²

ing deformations of the beam located at the fixed end were limited by the laboratory's reaction wall. The steel loading frame, attached to the movable end beam, provided the rigid condition to this boundary element. Specimens UP2 and UP3 (Fig. 2) were tested to study a more flexible boundary condition because the hollow-core slabs could be influenced by the flexible response of the lateral beams. Topped specimen TP3 was tested with hollow-core slabs running parallel to the cyclic demand. Based on test site restrictions, the specimens were constructed using two 1200 mm wide × 2980 mm long × 100 mm deep (47 × 117 × 4 in.) hollow-core slabs. Specimens built with three hollow-core slabs included an intermediate 1000 mm (40 in.) wide hollow-core slab.

The bearing length for the hollow-core slabs was 50 mm (2 in.), according to ACI 318-14.[13] The height for the fixed end and lateral beams was 300 mm (12 in.). For the beam located at the movable end, the height was 500 mm (20 in.) to accommodate the load bearing. To represent the influence of the continuity of the diaphragm beyond the limits of the test specimens and to avoid the formation of mechanisms affecting the response of the corner beam joints, the perimeter beams located at the fixed and movable ends were extended 300 mm beyond the joints. All perimeter beams were cast in two stages: a 200 mm (8 in.) deep precast concrete portion reinforced longitudinally with four 12 mm (no. 4) bars and a 100 mm (4 in.) thick cast-in-place concrete portion with two additional 12 mm longitudinal bars. Horizontal shear resistance and continuity with the cast-in-place concrete were provided by 10 mm (no. 3) transverse closed stirrups that emerged from the precast concrete section. The cast-in-place concrete portion of the perimeter beams was cast at the same time as the joints and connections of the hollow-core slabs. The connection detail between the hollow-core slabs and the perimeter beams consisted of 10 mm hooked reinforcing bars. These connectors were designed to contribute to shear resis-

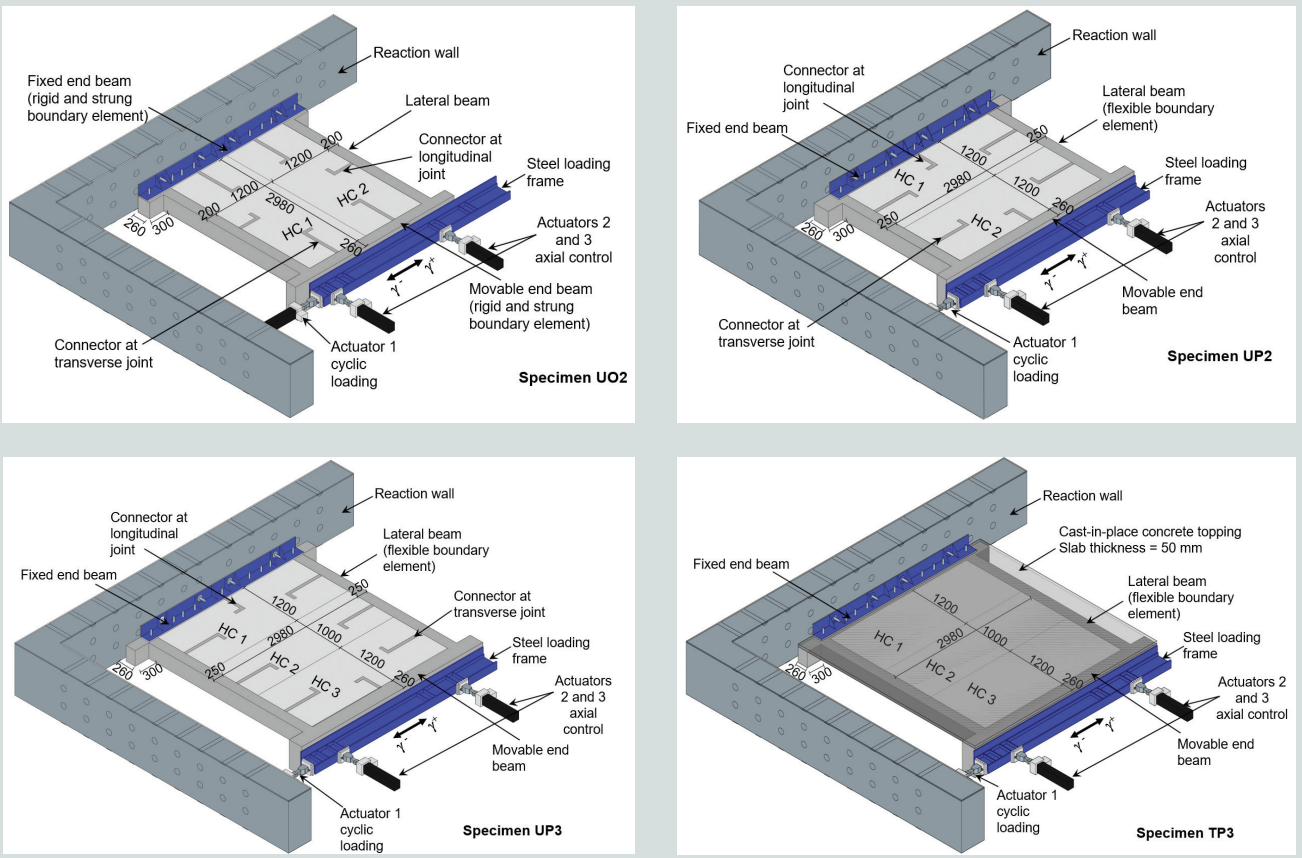

Figure 2. Test specimen and setup schematics. Note: All dimensions are in millimeters. 1 mm = 0.0394 in.

tance through shear friction mechanism[14] and also served as structural integrity reinforcement. The connectors were placed in the central cores, which were previously broken out at each hollow-core unit end. These cores were then filled with concrete. This connection detail is widely used in untopped hollow-core diaphragms and is documented in other design guidelines.[14,15] The tie connector details included 90- and 180-degree end hooks within the hollow-core slabs and the supporting beams, respectively. The connectors were developed within the filled cores at a distance equal to the transfer length of the pretensioned tendons in the hollow-core units, that is 720 mm (28 in.).[16] Tie connectors across the longitudinal joint, between the perimeter beams and hollow-core slabs, were located at the midspan of the precast concrete units. For specimen TP3, which had a 50 mm (2 in.) thick cast-in-place concrete topping, composite action between the topping and the hollow-core slabs was established. Thus, the surfaces of the hollow-core slabs were intentionally roughened with a minimum depth of 6 mm (0.25 in.) in a bidirectional pattern.[13] Welded-wire reinforcement with a 5.0 mm (0.2 in.) diameter and 250 × 250 mm (10 × 10 in.) spacing was used for the topping slab reinforcement, which satisfied requirements for minimum spacing and resisted shrinkage- and temperature-induced volumetric changes.[13]

A bidirectional test fixture was developed to allow simultaneous control of in-plane lateral loading and bending deformations of the specimen through the use of three actuators. **Figure 3** illustrates the test setup. The test specimens were connected and fastened to the laboratory reaction wall on the fixed end, while the beams located on the movable end rested vertically on two polytetrafluoroethylene-based pads, providing freedom of horizontal movement with minimal friction force. The actuators were connected through a steel loading frame to the free end of each specimen. The steel loading frame was anchored to the concrete beams through twelve 32 mm (1.25 in.) diameter post-tensioning bars. The test setup did not account for other types of demands or mechanisms that could be developed in the elements of the lateral-force-resisting system that could affect the behavior of the diaphragm system.

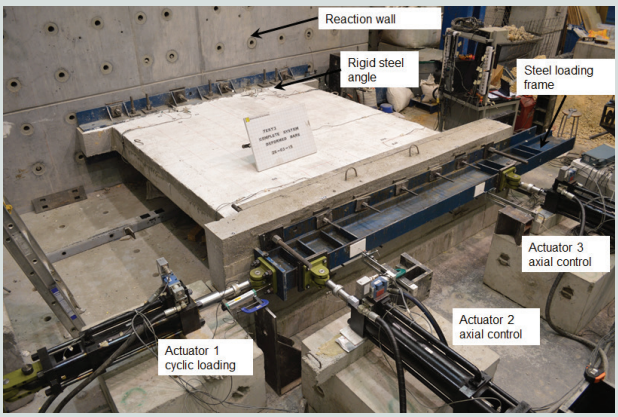

Figure 3. Typical test setup used in the experimental program.

Materials

The specified concrete strength for the hollow-core slabs was 60 MPa (8.7 ksi). The average measured compressive strength of the concrete used for the cast-in-place portion of the perimeter beams, longitudinal joints, and to fill the broken-out cores, corresponding to the day of the test, was 25 MPa (3.6 ksi). All reinforcing steel was specified as 414 MPa (ASTM A706 Grade 60) with a minimum yield strength of 420 MPa (60 ksi). Based on test results, the average yield strain was 2.6 mm/mm. This steel was also used for the 10 mm (no. 3) tie connectors. The welded-wire reinforcement used in specimen TP3 was specified as 448 MPa (ASTM A1064 Grade 65) with a minimum yield strength of 485 MPa (70 ksi).

Instrumentation

The specimens were instrumented with different types of sensors to monitor and record forces, displacements, and strains. Three 445 kN (100 kip) capacity load cells (one per actuator) were used to monitor the applied forces to the test specimens by the hydraulic actuators. Displacement transducers were used at the mid-longitudinal joints to capture the relative sliding between adjacent hollow-core slabs and between the hollow-core slabs and the perimeter beams. A series of displacement transducers was also used to measure the opening across the transverse joints. These gauges helped to determine the deformation of the hollow-core slabs relative to the perimeter beams. Strain gauges were attached to tie connectors of the untopped specimens to monitor the deformation history through the tests.

Test protocol and control

To properly represent the boundary conditions of the subdiaphragm region used in this research, displacement control and force control were implemented. The displacement control corresponded to a cyclically increasing demand protocol applied through actuator 1. This cyclic test protocol was in accordance with the recommendations set forth by the PRESSS (Precast Seismic Structural Systems) program for subassemblages, where the definition of a reference deformation based on ductility is inappropriate.[17] The cyclic test protocol consisted of groups of three symmetric cycles at increasing levels of shear distortion, calculated as the following:

$$\gamma = \Delta / L_c$$

where

Δ = the horizontal displacement measured at the middle of the cross section of the movable end beam

L_c = the center-to-center distance between the fixed end and movable end beams

The cyclic shear distortion protocol implemented through actuator 1 was conducted at quasi-static rates (1.27 mm/sec

[0.05 in./sec]). **Table 2** gives the sequence of shear distortions and the corresponding displacements for each test. A force-based control was used for actuators 2 and 3. Once each shear distortion substep was applied, the force in actuator 1 was measured. Subsequently, actuators 2 and 3 applied forces in opposite directions such that the moment induced by actuator 1 was balanced.

Experimental results and discussion

Test observations

Despite the differences in the boundary conditions, the damage pattern evolution of the untopped specimens exhibited comparable behavior. In general, the untopped specimens exhibited pretest shrinkage cracking at the interfaces between the cast-in-place concrete and the hollow-core slabs along the transverse and longitudinal joints. The maximum pretest crack registered was approximately 1.0 mm (0.04 in.) wide.

Figures 4 through **6** show the damage evolution of the untopped specimens for selected shear distortion amplitudes. The overall behavior of the untopped specimens (UO2, UP2, and UP3) was described by an initial cracking pattern along the longitudinal and transverse joints up to shear distortions of approximately 0.15%. The initial cracking was followed by incipient concrete spalling along the longitudinal joints between the hollow-core slabs for an approximate shear distortion of 0.20%. Once concrete spalling extended along the longitudinal joints ($\gamma = 0.25\%$), a gradual opening across the transverse joints was observed, likely due to the rocking behavior of the hollow-core slabs with respect to the supporting beams. Simultaneously, the development of vertical cracks on the external faces of the supporting beams was observed in the untopped specimens UP2 and UP3 with more flexible conditions (Fig. 5 and 6). This crack pattern was not detected in the specimen with the upper-bound condition UO2 because in-plane flexural deformations of the supporting beams were constrained. For the untopped specimen UP3, the longitudinal

Table 2. Cyclic test protocol: target shear distortions and displacements

Shear distortion γ, %	Target displacement Δ			
	UO2, mm	UP2, mm	UP3, mm	TP3, mm
0.05	1.57	1.34	1.84	1.84
0.075	2.35	2.01	2.76	2.76
0.10	3.13	2.68	3.68	3.68
0.15	4.7	4.01	5.51	5.51
0.20	6.26	5.35	7.35	7.35
0.25	7.83	6.69	9.19	9.19
0.35	10.96	9.36	12.86	12.86
0.50	15.65	13.38	18.38	18.38
0.75	23.48	20.06	27.56	27.56
1.00	31.3	26.75	36.75	36.75
1.50	46.95	40.13	55.13	55.13

Note: 1 mm = 0.0394 in.

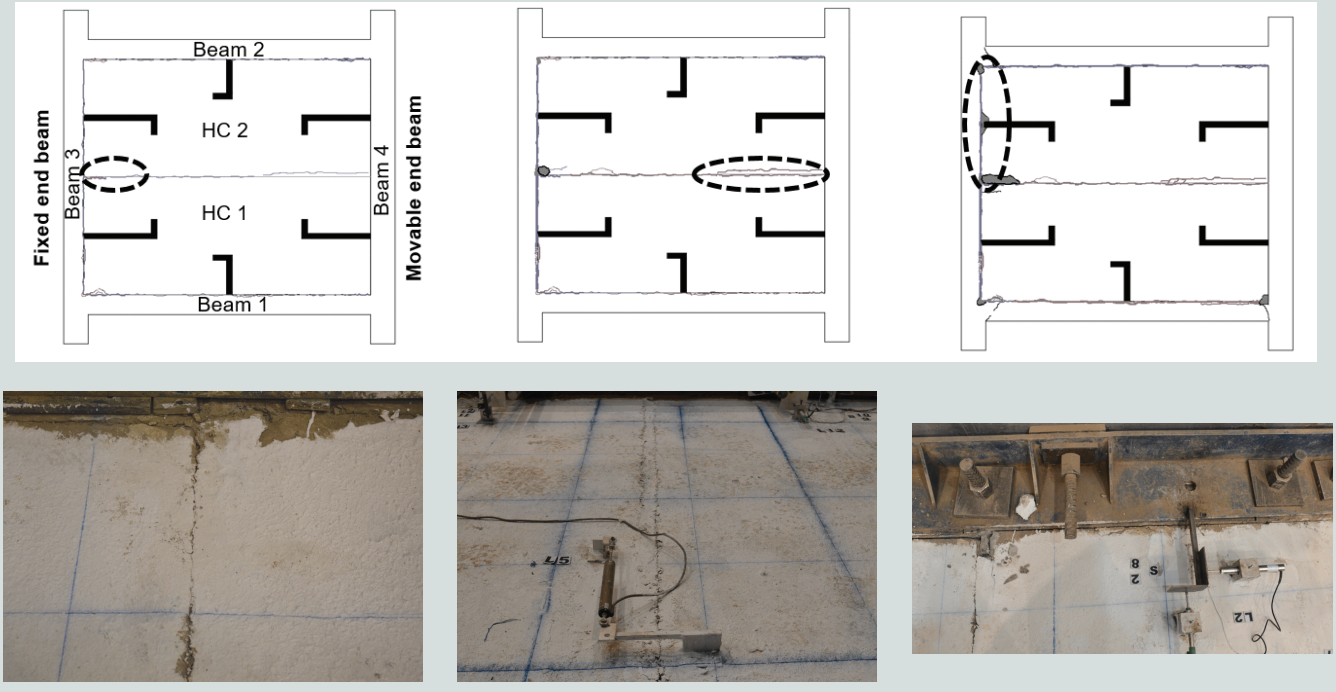

Figure 4. Progressive damage pattern for untopped specimen UO2.

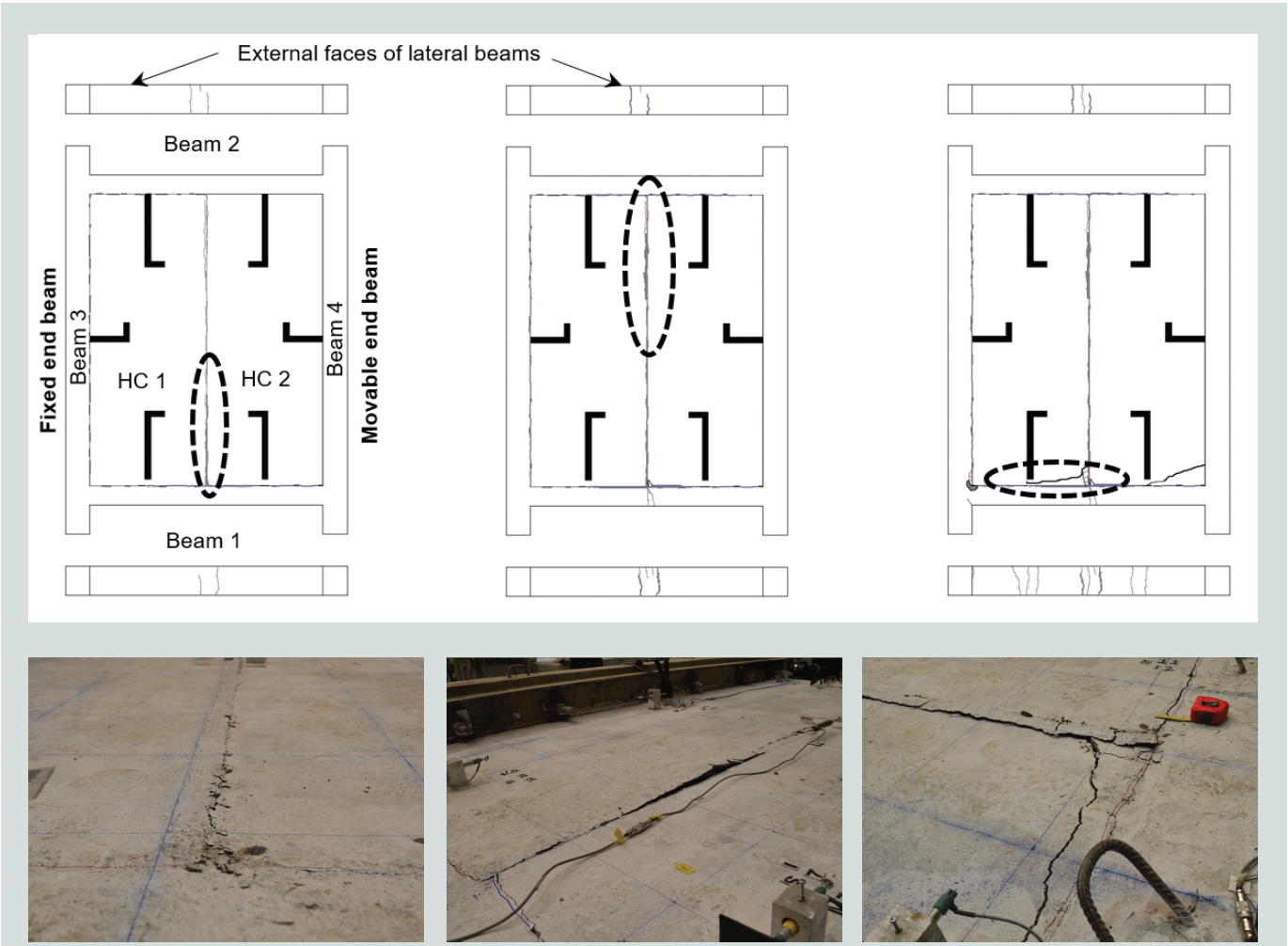

Figure 5. Progressive damage pattern for untopped specimen UP2.

joint between hollow-core slabs 1 and 2 remained uncracked, concentrating the slip along one joint. For higher levels of shear distortion amplitudes ($\gamma > 0.35\%$), the concentrated stresses at the hollow-core slab corners reacting against the perimeter beams caused accumulated damage at these locations. Crushing and diagonal fracture of the corners of the hollow-core slabs were observed at these stages. It should be noted that a failure in the test control occurred during the application of the first negative cycle for $\gamma = 1.0\%$ for test specimen UP2, significantly affecting the performance for subsequent cycles.

Specimen TP3, which incorporated a 50 mm (2 in.) topping, exhibited a crack pattern on the cast-in-place concrete topping near the longitudinal joint between hollow-core slab 1 and the fixed end beam (**Fig. 7**). Propagation and widening of the cracks were observed during the test up to $\gamma = 0.25\%$. For subsequent cycles, the concentrated damage to the cast-in-place concrete topping was related to the fracture and even dislocation of the topping slab. This could have induced high strain demands on the topping reinforcement. During the application of the cyclic loading for shear distortion levels $\gamma = 0.75\%$ and $\gamma = 1.0\%$, fracture of the welded-wire reinforcement was detected. No damage to either the hollow-core slabs or the joints was reported.

The overall performance of untopped and topped specimens differed from each other because the untopped specimens exhibited a widespread damage pattern, particularly along the joints and at the corners of the hollow-core slabs. The cracking pattern of the untopped specimens corresponded primarily to the expected cracks at the interfaces between the hollow-core slabs and the cast-in-place concrete of the perimeter beams. These interfaces prompted a separation (opening) between the precast concrete units and the perimeter beams due to the jointed nature of the untopped system. In contrast, the topped specimen showed concentrated and substantial damage to the cast-in-place concrete topping close to the rigid support. This localized damage generated large strain demands and, subsequently, the fracture of the topping reinforcement. The cracking pattern of the topped specimen differed from the untopped systems in that it corresponded entirely to damage to the cast-in-place concrete layer, whereas most of the cracks reported for the untopped specimens corresponded to openings across the joints caused by concrete cast at different times.

Responses of the specimens

Overall specimen performance was assessed through hysteresis loops, observed performance, and measured data. **Figure 8** shows the complete force-shear distortion hysteresis curves and envelopes from the test results. **Figure 9** details of the behavior within the expected range of shear distortion for hollow-core diaphragms for values of $\gamma \leq 0.25\%$. This value of shear distortion was established based on the results of nonlinear numerical models of complete (whole building) diaphragms under seismic loads.[18] Opening contact measurements across transverse joints between the hollow-core slabs and the perimeter beams were used to calculate the rigid body rotation of the hollow-core slabs. This rotation was calculated as the difference between the displacement measured by adjacent transducers across transverse joints within a hollow-core slab divided by the distance between the instruments. Secant stiffness degradation was also calculated to relate it to the previously described damage pattern. The secant stiffness of each cycle was calculated as the ratio between the difference in peak forces in each direction and the difference in the corresponding lateral displacements associated with a shear distortion.

Untopped specimen UO2 Up to a shear distortion of 0.15%, the hysteretic loops exhibited early nonlinear behavior (Fig. 9) mainly due to the gradual opening across the transverse joints. For these stages, peak forces for negative shear distortions were 38% greater on average than those achieved for positive shear distortions. This phenomenon was associated with the higher slip between the hollow-core slabs along the longitudinal joint toward the positive shear distortion. This behavior could indicate that there was a higher shear strength along the longitudinal joint for positive shear distortions. As the test continued, the hysteresis curve showed stable behavior of the specimen, with an increasing strength trend up to $\gamma = 0.25\%$. At this level, differences between positive and negative peak forces (Fig. 9) reduced to 11.5%. An early pinching of the hysteretic loops was observed because of the residual opening in the transverse joints during reloading. Thus, once the gaps across the transverse joints were closed, an increase in both stiffness and strength was detected in the hysteretic loops.

At the end of the cyclic loading for $\gamma = 0.25\%$, an emerging and localized spalling of the cast-in-place concrete along the longitudinal joint was observed, accompanied by rotation of the hollow-core slabs and early crushing of the interior corner of the hollow-core slabs at the fixed end beam. This was likely due to the rocking behavior of the hollow-core slabs. From the kinematics of the hollow-core slabs, it appeared that a resistance mechanism developed between the opposite corners of the hollow-core slabs, forming a diagonal strut (**Fig. 10**). Based on the previous consideration, the initial trend can be characterized by the shear resistance along the longitudinal

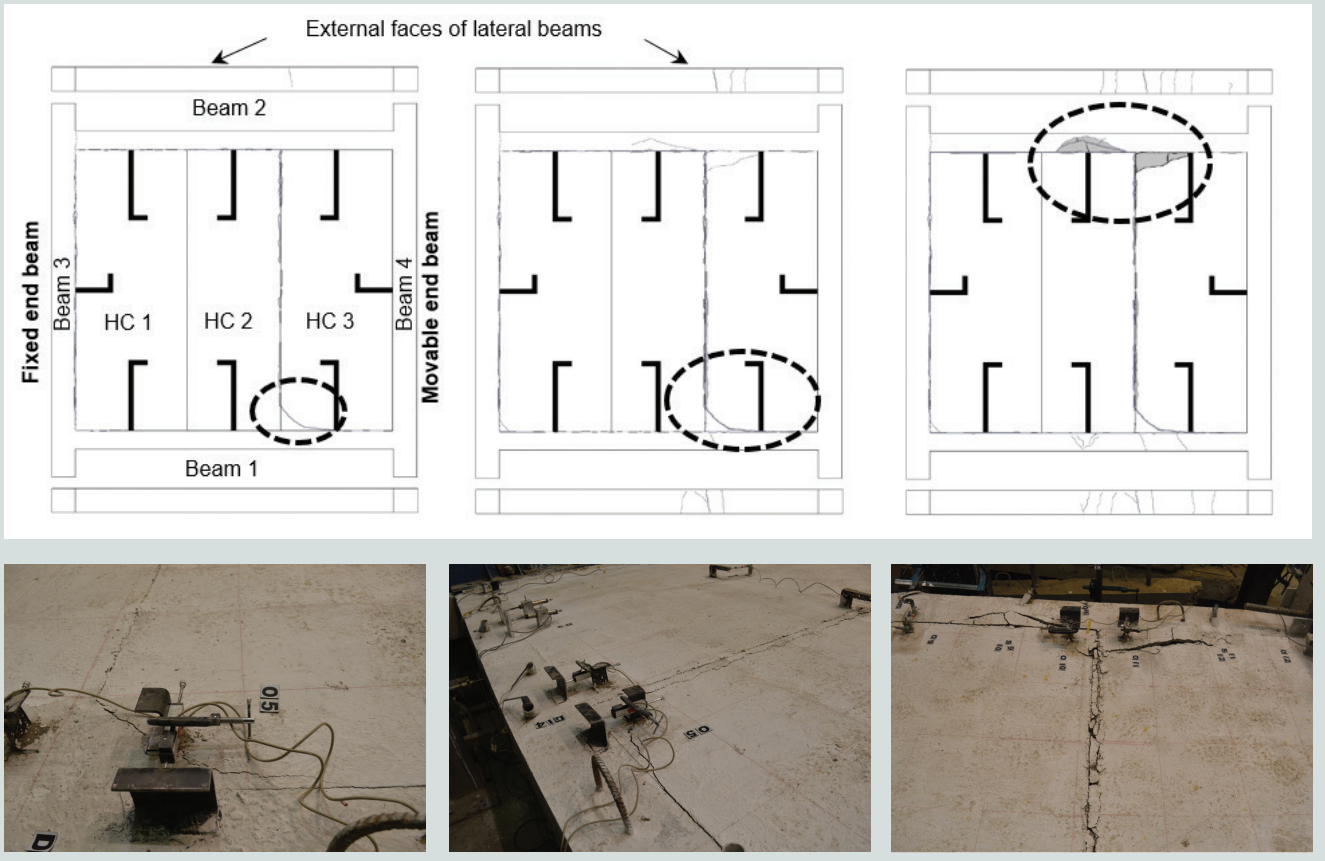

Figure 6. Progressive damage pattern for untopped specimen UP3.

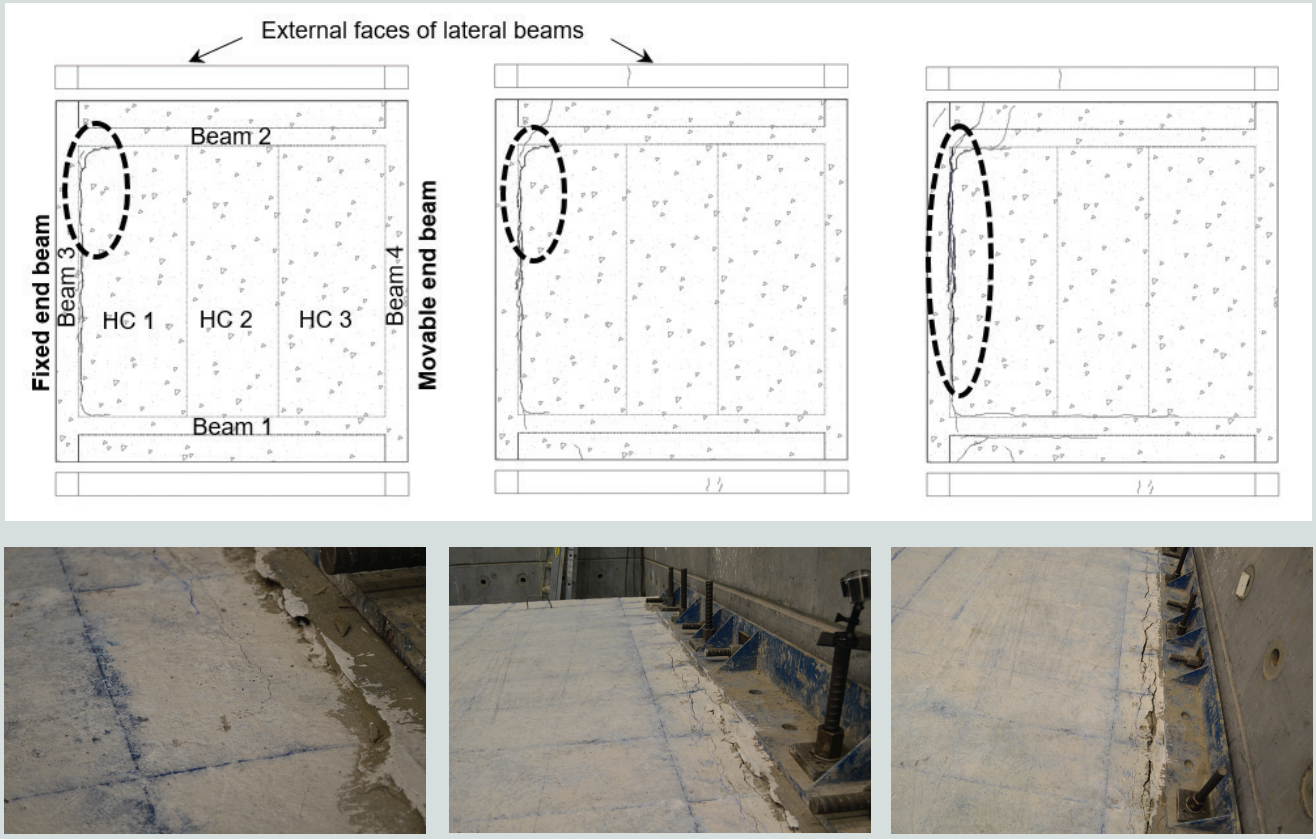

Figure 7. Progressive damage pattern for topped specimen TP3.

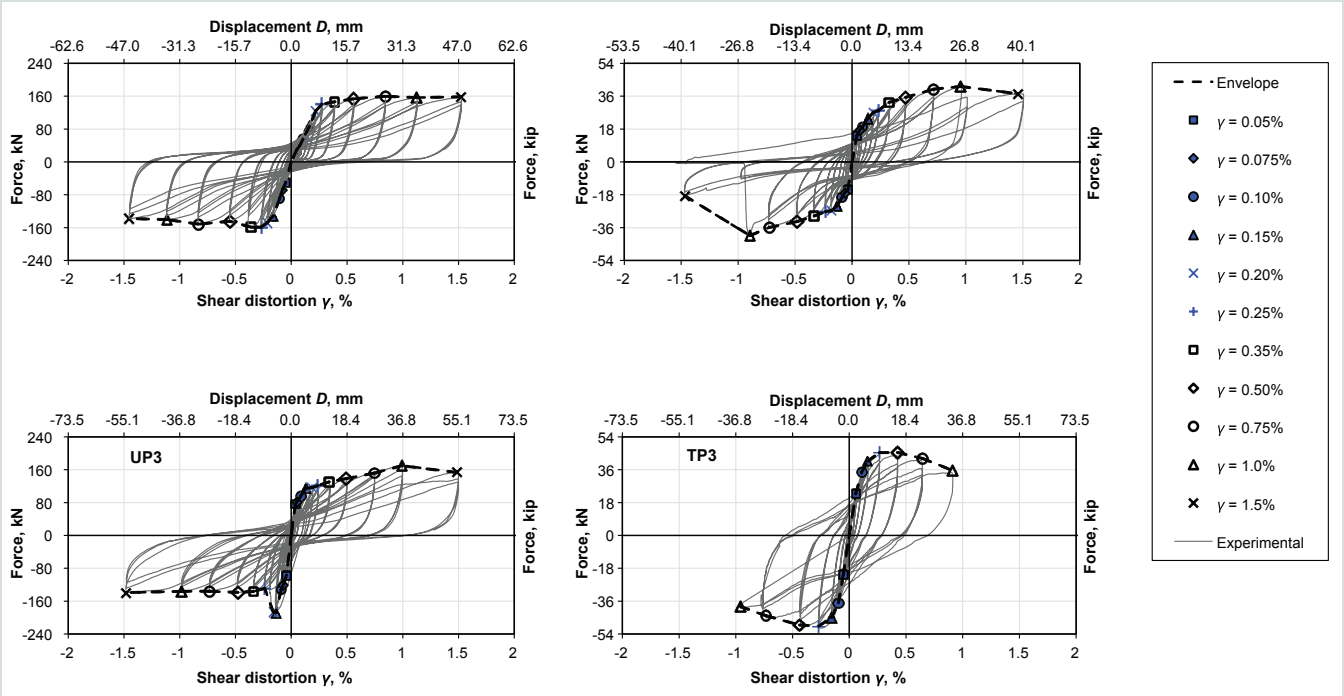

Figure 8. Force-shear distortion hysteretic loops and envelopes: overall response. Note: 1 mm = 0.0394 in.

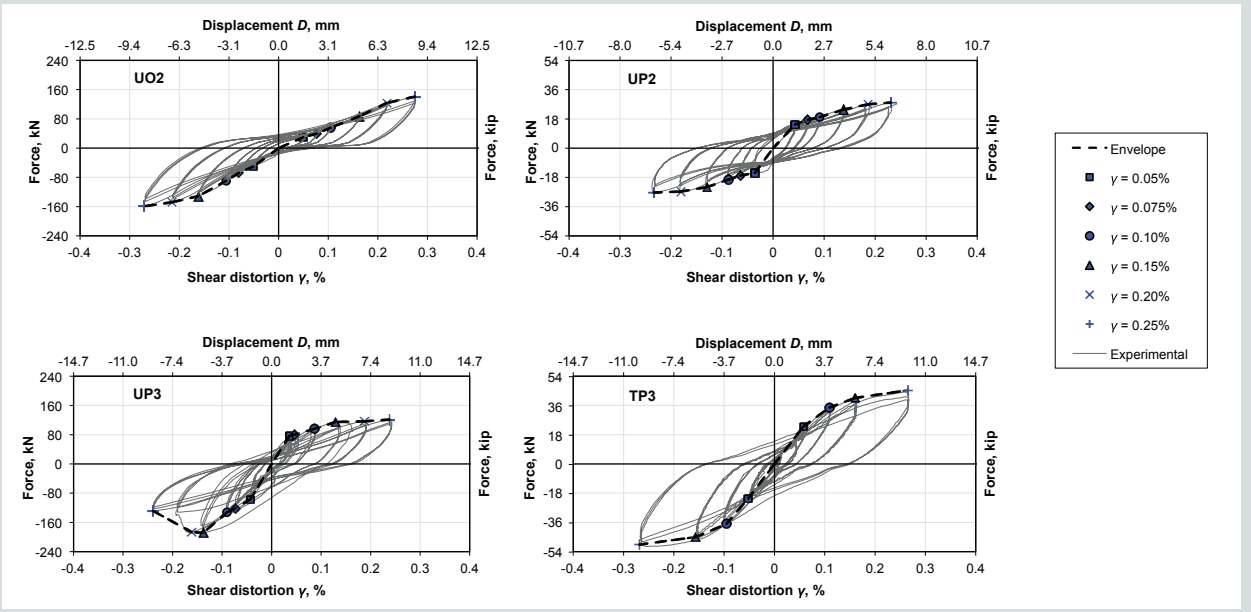

Figure 9. Force-shear distortion hysteretic loops and envelopes: initial response. Note: 1 mm = 0.0394 in.

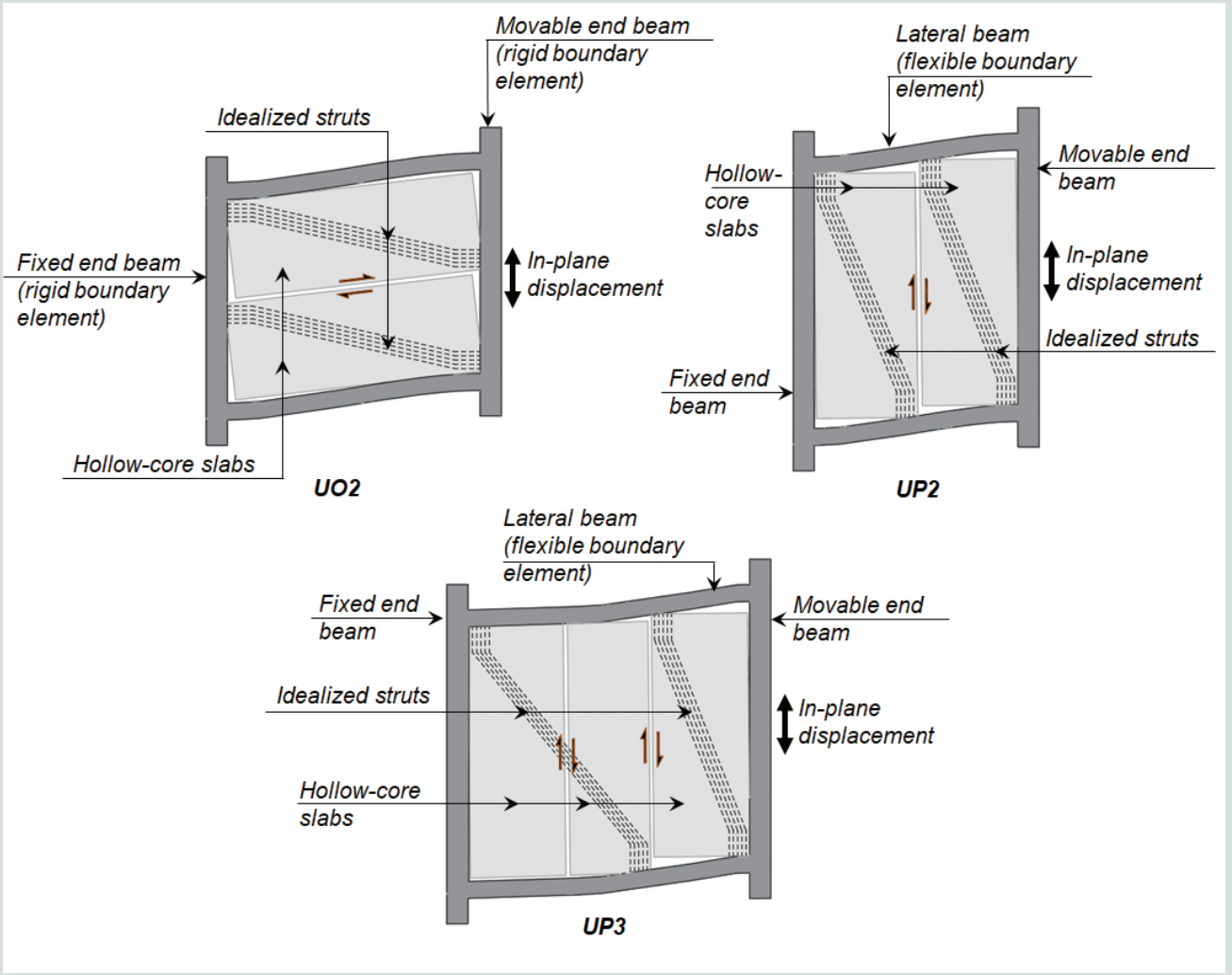

Figure 10. Scheme of the strut mechanism developed within hollow-core slabs in untopped specimens.

Table 3. Measured maximum axial strains at tie connectors across longitudinal and transverse joints for untopped specimens

Shear distortion γ, %	Axial strain, mm/mm × 10^{-3}					
	UO2		UP2		UP3	
	Transverse joint	Longitudinal joint	Transverse joint	Longitudinal joint	Transverse joint	Longitudinal joint
0.05	0.48	0.20	0.52	0.30	0.00	0.01
0.075	0.73	0.30	0.61	0.30	0.01	0.01
0.10	0.97	0.40	0.71	0.30	0.01	0.01
0.15	1.60	0.70	1.31	0.50	0.03	0.05
0.20	2.06	0.80	1.80	0.50	2.31	0.05
0.25	2.30	0.80	2.04	0.60	2.66	0.03
0.35	8.45	0.90	3.50	0.80	4.35	0.03
0.50	12.16	1.20	6.81	1.20	19.19	0.04
0.75	13.72	2.10	10.20	2.40	17.24	0.05
1.00	4.49	1.40	10.59	11.90	15.43	0.10
1.50	4.30	3.50	12.90	3.30	14.90	0.20

Note: Yield strain = 2.6 mm/mm × 10^{-3}. 1 mm = 0.0394 in.

joints and the possible contribution of the diagonal elastic struts that could develop within each hollow-core slab.

For shear distortions greater than 0.25% (Fig. 8), the test specimen exhibited nearly constant strength. Further crushing on the corners of the hollow-core slabs was reported for subsequent stages. The concentrated damage at the corners of the hollow-core slabs caused by bearing stresses may confirm the previously explained diagonal strut mechanism. For shear distortions greater than 0.25%, the hysteresis curve and the reported damage might have indicated plastic behavior of the diagonal strut mechanism. **Table 3** shows that the connector across transverse joints with the greatest demand exceeded its yield strain during the application of the cyclic loading for γ = 0.35%. From the measured joint opening used to calculate the rotations of the hollow-core slabs, it appears that most of the tensile strains reported for these connectors corresponded to the control of the transverse joint opening, though contribution to the resistance by shear-friction mechanism also demanded tensile strains on the connectors. Connectors across longitudinal joints exhibited significant lower values of strain compared to those measured across transverse joints.

Figure 11 shows a strong correlation between the applied shear distortions and the rigid body rotation of the hollow-core slab. Furthermore, both the positive and negative rotations induced in the hollow-core slabs were of the same order as the applied shear distortions. **Figure 12** shows the variation of the secant stiffness with the shear distortion for each of the three cycles that comprise the cyclic test protocol per shear distortion. Initial secant stiffness degradation (11.5%) was related to the initial cracking along the transverse joint at the fixed end beam. For the cycles corresponding to shear distortions between 0.075% and 0.1%, a low secant stiffness degradation was detected because there was no evidence of significant cracking on the specimen. After the application of the second cycle for a shear distortion of 0.15%, an evident trend in the secant stiffness degradation was observed as cracking and spalling of the concrete along the longitudinal joint occurred. Most of the secant stiffness degradation occurred between γ = 0.15% and γ = 0.50%. For further cycles of the test protocol (γ > 0.50%) the secant stiffness degraded at a lower rate because of the accumulated damage to the hollow-core slab corners. At the end of the test, a secant stiffness degradation was 89%.

Untopped specimen UP2 Figure 9 shows that for γ = 0.05%, the specimen exhibited a visible amplitude of the hysteretic loop due to the early opening and closure of the cracks along the transverse joints. There was a considerable drop of the lateral stiffness caused by incipient spalling along the longitudinal joint between the hollow-core slabs reported during the application of the test protocol for γ = 0.075% and γ = 0.10%. Thus, the initial stiffness highly depended on the response of the longitudinal joint between the hollow-core slabs.

After the cyclic loading for γ = 0.15% was completed, the system stiffness dropped 41% because of the continued concrete spalling along the longitudinal joint and the extension of the existing cracks. As the longitudinal joint slip became more evident, it was observed that bearing stresses developed between the corners of the hollow-core. As previously

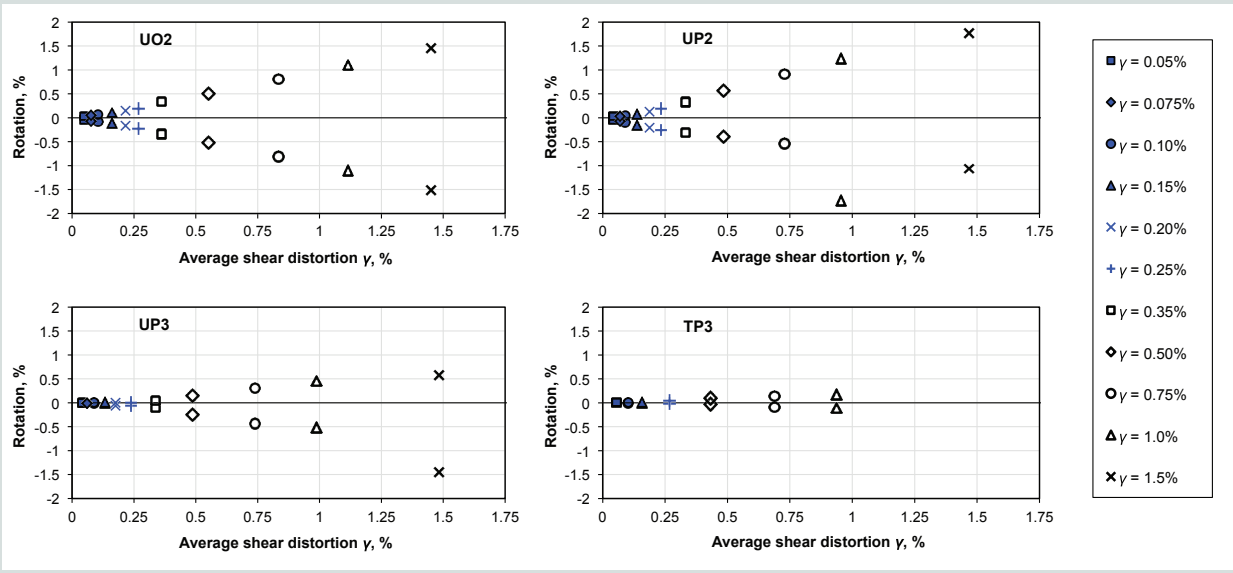

Figure 11. Maximum rotation of hollow-core slabs per shear distortion.

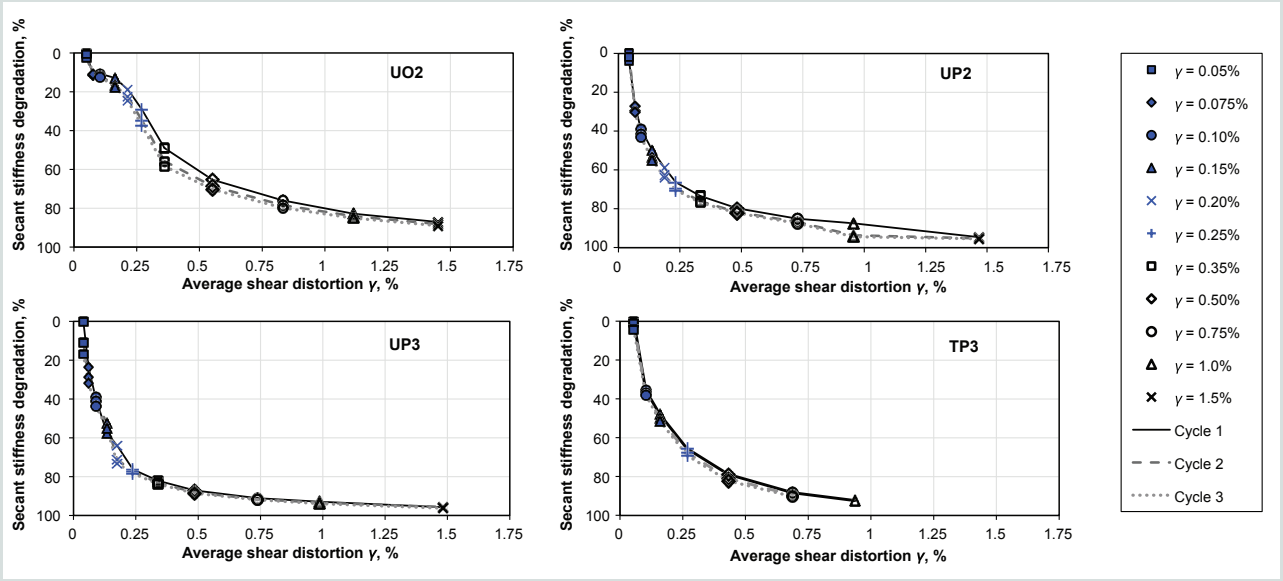

Figure 12. Secant stiffness degradation calculated for test specimens.

explained, these bearing stresses at opposite corners can resemble the formation of a diagonal strut resistance mechanism developed within the hollow-core slabs (Fig. 10). Furthermore, due to the boundary conditions of the supporting framing beams, the formation and gradual opening of vertical cracks at the midspan of perimeter beams 1 and 2 was detected when the interior corners of the hollow-core slabs developed bearing stresses against the supporting beams (Fig. 5). Thus, it can be argued that before significant concrete spalling occurred along the longitudinal joint, the increasing strength trend for $\gamma \leq 0.25\%$ may be associated with the contribution of both shear resistance along the longitudinal joints and the formation of the diagonal elastic strut mechanism between the opposite corners of the hollow-core slab. For subsequent shear distortion amplitudes, specimen UP2 showed an increase in lateral strength with reduced stiffness. The reduction in lateral stiffness was related to the accumulated damage along the longitudinal joints, whereas the increase in lateral strength could be determined by the resistance mechanism attributed to the diagonal struts.

The fracture of hollow-core slab 2 at the first negative cycle during the application of the test protocol for $\gamma = 0.75\%$ was followed by a pinching of the hysteresis loops for the next two cycles in that direction. The failure in the test control during the first negative cycle for $\gamma = 1.0\%$ caused evident damage that affected stiffness and strength for subsequent negative cycles (Fig. 8). For further positive shear distortion demands,

the test specimen exhibited nearly constant strength due to the increasing opening measured at the transverse joints and damage to the hollow-core slabs. Table 3 summarizes the maximum strains measured in the tie connectors of specimen UP2 across transverse and longitudinal joints. The tie connector across transverse joints with the greatest demand achieved its yield strain for $\gamma = 0.35\%$. Similar to the results for specimen UO2, a correlation between the observed transverse joint opening and tensile strains obtained at these locations might explain that most of the strains corresponded to a clamping effect between perimeter beams and hollow-core slabs due to opening of the transverse joints. Connectors across longitudinal joints exhibited significantly lower strain values compared with those measured across transverse joints. Because of the high demand on the specimen as a consequence of the failure in test control for $\gamma = 1.0\%$, strain in connectors across longitudinal joints exhibited unrestricted yielding.

The correlation between the calculated hollow-core rotation and the average induced shear distortion (Fig. 11) shows a strong linear dependence between both variables up to $\gamma = 0.75\%$. Negative hollow-core rotation for $\gamma = -1.0\%$ was affected by the failure in the test control. The average rotations calculated for the hollow-core slabs were slightly lower than the applied shear distortions. Figure 12 shows the degradation of the secant stiffness with shear distortion for each cycle. Although higher values of secant stiffness at each stage were obtained for the first cycle, there were no substantial differences between cycles. The initial secant stiffness degraded nearly 30% due to the early damage to the longitudinal joint between hollow-core slabs. At the end of the cyclic loading for $\gamma = 0.20\%$, the accumulated secant stiffness degradation was approximately 64%. This stiffness degradation was related to the cracking and concrete spalling along the longitudinal joint between the hollow-core slabs. Once concrete spalling was evident along this joint ($\gamma > 0.25\%$), the secant stiffness degraded at a lower rate.

The fracture of the hollow-core slab during the implementation of the cyclic test protocol for $\gamma = 0.75\%$ did not significantly affect the secant stiffness of the specimen. Failure in test control during the application of cyclic test protocol for $\gamma = 1.0\%$ is noted in the degradation for the second and third cycles. At the end of the test, the secant stiffness degradation was 95%.

Untopped specimen UP3 Up to a shear distortion of 0.10%, peak forces for negative shear distortions were 27% greater on average than those achieved for positive shear distortions. During the application of the cyclic test protocols for $\gamma = 0.15\%$ and $\gamma = 0.20\%$, this difference between peak forces increased up to 38%. Increase of the negative lateral stiffness from $\gamma = 0.10\%$ to $\gamma = 0.15\%$ was also observed. For these early stages (Fig. 9), the hysteresis curve showed a more rigid and wider loop response during the negative reloading path.

After the peak force was achieved for the first negative cycle during the implementation of the test protocol for $\gamma = 0.20\%$, fracture of hollow-core slab 3 in contact with perimeter beam 1 occurred (Fig. 6). The lateral force dropped significantly (31%) for subsequent cycles. This early fracture seems to have been caused by a stress concentration between hollow-core slabs 2 and 3 generated by the horizontal shear that developed along the longitudinal joint, affecting the response of the specimen for negative shear distortion demands. The longitudinal joint between hollow-core slabs 1 and 2 remained uncracked with almost zero slip. Due to the fracture of hollow-core slab 3 and the exhaustion of shear strength along the longitudinal joint between hollow-core slabs 2 and 3, the rotation calculated for hollow-core slab 3 exhibited an increasing trend for further shear distortion amplitudes (Fig. 11). This behavior led to the bearing mechanism developed through diagonal struts between the opposite corners of the hollow-core slabs (Fig. 10). Due to the flexible boundary condition of the supporting framing beams, this diagonal strut appeared to trigger the opening of the cracks observed along the span of these beams (Fig. 6). Thus, the initial behavior appears to have been influenced by the shear resistance along the longitudinal joints and the diagonal strut mechanism within hollow-core slab 3 and within hollow-core slabs 1 and 2 acting as a unit.

As the test continued, lateral negative stiffness decreased significantly, showing a nearly constant strength trend. Figure 8 shows that the positive branch (y-axis) exhibited an increasing strength trend with reduced stiffness up to $\gamma = 1.0\%$. For $\gamma > 0.20\%$, a progressive pinching effect was observed on the hysteresis curve because of the residual opening in the transverse joints during reloading.

Table 3 gives the maximum strains reported in the tie connectors across transverse and longitudinal joints for specimen UP3. The connector across transverse joints with the greatest demand exceeded its yield strain for $\gamma = 0.25\%$. Similar to the results for specimens UP2 and UO2, tensile strains on tie connectors across transverse joints appeared to be controlled by the clamping effect between the perimeter beams and the hollow-core slabs. In general, the tie connector across the longitudinal joints between hollow-core slabs and perimeter beams showed very small levels of strain during the test.

Figure 11 shows the strong correlation between the applied shear distortions and the rigid body rotation of hollow-core slab 3. In this case, the rotation of hollow-core slab 3 corresponded to nearly half of the applied shear distortions. The secant degradation shown in Fig. 12 indicates that despite the higher values of secant stiffness at each stage that were obtained for the first cycle, there were no substantial differences between cycles. For the first cycle, the secant stiffness degradation up to $\gamma = 0.20\%$ was approximately 64% and was mainly related to cracking and initial concrete spalling along the longitudinal joint between hollow-core slabs 2 and 3. The fracture of hollow-core slab 3 during the cyclic loading for $\gamma = 0.20\%$ induced a drop-off in the secant stiffness degradation for the second and third cycles for this shear distortion level. For $\gamma > 0.25\%$, the secant stiffness degraded at a lower rate. The second fracture of hollow-core slab 3 during the imple-

mentation of the cyclic loading for $\gamma = 0.50\%$ and the splitting failures of the tie connectors of hollow-core slab 2 did not significantly affect the secant stiffness of the specimen. At the end of the test, secant stiffness degradation was 96%.

Topped specimen TP3 Figure 9 shows a nearly symmetric hysteretic response in the early stages. An average difference of 8% between peak force responses for negative and positive shear distortions was calculated up to $\gamma = 0.25\%$. Early hysteretic behavior could be attributed to the increasing cracking along the longitudinal joint at the fixed end that demanded high strains in the welded-wire mesh reinforcement. There was also a decrease in lateral stiffness between $\gamma = 0.10\%$ and $\gamma = 0.25\%$ caused by the progressive cracking. A measured residual crack width of 1.8 mm (0.70 in.) at the end of the cyclic loading for $\gamma = 0.25\%$ indicated that fracture of the concrete topping occurred.

The peak force for negative shear distortions was achieved during the application of the cyclic loading for $\gamma = 0.25\%$. Figure 8 shows that for shear distortions between 0.25% and 0.50%, the test specimen exhibited nearly constant strength as the fracture on the concrete topping slab extended and widened along the fixed end longitudinal joint. At the end of the cyclic loading for $\gamma = 0.50\%$, the maximum residual width of the fractured portions of the cast-in-place topping was 3.0 mm (0.12 in.). The peak force for positive shear distortions was achieved for $\gamma = 0.50\%$, which is not substantially different from the peak force achieved for $\gamma = 0.25\%$. The nearly constant strength for $0.25\% < \gamma \leq 0.50\%$ indicates that the strength capacity was limited by the fracture of the cast-in-place concrete topping. For further increments of shear distortion, the test specimen exhibited strength degradation caused by the propagation of the concrete topping fracture, achieving levels of dislocation. This damage led to the fracture of the welded-wire reinforcement.

Figure 11 shows that once concrete topping dislocation occurred for $\gamma \geq 0.50\%$, rotation of hollow-core slab 1 exhibited an increasing trend. These results and the small values of slip along the longitudinal joints between hollow-core slabs for shear distortions up to $\gamma = 0.25\%$ indicated that the hollow-core slabs were adequately jointed by the cast-in-place concrete topping. Once the fracture of the welded-wire reinforcement was reported during the implementation of the first cycle for $\gamma = 0.75\%$, the peak forces reduced by 7% and 11.4% for positive and negative shear distortions, respectively. With the concrete topping dislocation along the longitudinal joint for $\gamma = 1.0\%$, a second topping reinforcement wire fractured and the strength capacity was reduced by 22%.

Despite the stiffness and strength degradation caused by the nonductile failure mechanism, the specimen seemed to have good energy dissipation based on the amplitude of the hysteretic loops obtained from the early stages. Furthermore, the overall hysteretic behavior (Fig. 8) showed that the cyclic response of the topped specimen did not exhibit pinching of the loops. These results and observations indicated that the strength capacity of the system was highly affected by the behavior of the cast-in-place concrete topping slab because increase of strength capacity was limited by the fracture of the topping concrete and was followed by a degradation trend as the fracture of the topping reinforcement propagated.

Figure 11 shows the almost linear relationship between the applied shear distortions and the rigid body rotation of hollow-core slab 1. However, the magnitude of the rotation was low compared with those reported for the untopped specimens. For hollow-core slabs 2 and 3, the calculated rotations were very small.

Figure 12 shows the calculated degradation of the secant stiffness with the shear distortion. Although higher values of secant stiffness at each stage were obtained for the first cycle, there were no substantial differences between cycles. For the first cycles, an accumulated secant stiffness degradation of 72% was calculated up to $\gamma = 0.50\%$. Despite the accumulated cracking and fracture of the topping reinforcement for $\gamma \geq 0.75\%$, the secant stiffness degradation seems to follow an asymptotic trend for subsequent cycles. The secant stiffness degradation was 90% at the end of the test.

Comparison of results

The initial lateral stiffness of specimen UO2, representing the upper-bound condition, exhibited a reduced response compared with those obtained for the more flexible conditions of specimens UP2 and UP3. This was due to the kinematics of the upper-bound condition (UO2), which required the hollow-core slabs to rotate almost proportionally to the induced shear distortion (Fig. 11). In contrast, calculated rotations for the more flexible conditions represented by specimens UP2 and UP3 showed on average lower rotation demands on the hollow-core slabs for a given shear distortion. Thus, earlier cracking of the longitudinal and transverse joint openings affected the initial capacity of specimen UO2. Specimens UP2 and UP3 with the more flexible conditions did not exhibit the early pinching of the hysteretic response that was observed for the upper-bound condition because of the premature opening and closure of the gaps across the transverse joints.

For shear distortion $\gamma > 0.25\%$, there were no significant differences between the responses of the specimens with variations in the boundary conditions. Despite the damage to the corners of the hollow-core slabs (crushing and fracture) for $\gamma \geq 0.75\%$, untopped specimens with both rigid (UO2) and more flexible conditions (UP2 and UP3) were able to sustain the lateral force capacity for further increments of shear distortion. For large levels of shear distortion, cyclic behavior and progression of the damage to the untopped systems appeared not to be affected by the in-plane stiffness of the supporting beams.

The overall performance of untopped and topped specimens differed because the untopped specimens exhibited a spread pattern of the damage, particularly along the joints and at

the corners of the hollow-core slabs. In contrast, the topped specimen showed concentrated and substantial damage to the cast-in-place concrete topping close to the rigid support. This localized damage generated large strain demands and, subsequently, the fracture of the topping reinforcement.

In terms of measured responses, comparisons of the force-shear distortion envelopes of untopped and topped specimens (UP3 and TP3) demonstrated that the initial lateral stiffnesses were similar for both specimens, indicating a low influence of the cast-in-place concrete topping for low shear distortion demands. Despite the response of the specimen UP3 for negative shear distortion demands up to $\gamma = 0.15\%$ caused by the interaction between hollow-core slabs 2 and 3, topped specimen TP3 exhibited higher strength. The peak force for negative shear distortions was 7% greater than that of specimen UP3 and 30% greater for positive shear distortion demands. For intermediate shear distortion amplitudes ($\gamma = 0.25\%$ and $\gamma = 0.50\%$), the maximum forces reported for the topped specimen TP3 were on average 52% greater than those obtained for the untopped specimen UP3. Once cast-in-place concrete topping reinforcement fractures, the strength capacity of the topped system tended rapidly to match that of the untopped system. For $\gamma = 1.0\%$, the average difference in peak forces for this shear distortion level reduced to 8% because of the strength degradation in the topped specimen TP3. Thus, it appears that the strength capacity of the system was highly affected by the behavior of the cast-in-place concrete topping slab. Increase in strength was limited by the fracture of the concrete, whereas strength degraded as the fracture of the topping reinforcement propagated.

Despite the loss of shear strength along the longitudinal joints and the large openings experienced across the transverse joints that led to individual behavior of the precast concrete units, the untopped hollow-core systems redistributed stresses for large shear distortion demands and sustained the loads for large shear distortions compared with the topped specimen. This ability to redistribute stresses could be related to the performance of the idealized strut mechanism between the corners of the hollow-core slab. In the case of the topped specimen, the significant loss of strength associated with the nonductile performance of the topping reinforcement that led to the early end of the test did not indicate other mechanisms of redistribution related to the hollow-core slabs. However, the level of shear distortion for which fracture of the topping reinforcement led to a significant strength degradation (greater than 20%) could be overestimated for actual diaphragm demands. Consequently, the topped system could be expected to have better performance in terms of strength, stiffness, and damage control for shear distortions up to $\gamma = 0.50\%$.

Geometrical limitations of confining beams

The mechanism of in-plane shear transfer in this diaphragm system relies on the confinement provided by the beams. Thus, the confinement action can be lost if the beams lengthen sufficiently during an earthquake. Such lengthening will occur in beams of reinforced concrete moment-resisting frames and is amplified when plastic hinges develop.[19–21] As described previously, the confining beams in the test program described herein did not develop plastic hinges. This prompted the use of fundamental principles and engineering judgement to establish geometrical limitations for the confining beams that also act as beams in such frames. The underlying philosophy is that the diaphragm will not compromise the development and the deformation capacity of the inelastic lateral system mechanism.

Restrepo-Posada et al.[19] proposed the following expression to calculate the beam lengthening δ_{el} in beams of reinforced concrete moment resisting frames that develop positive and negative plastic hinges,

$$\delta_{el} = 2\theta_f \frac{l_b'}{l_{ph}}\left(d - d'\right) \tag{1}$$

where

θ_f = interstory drift angle

l_b' = clear beam span

l_{ph} = distance between positive and negative beam plastic hinges within the beam span

d = effective beam depth

d' = distance from the extreme fiber in compression to the centroid of the compression reinforcement

Equation 1 can be simplified assuming $d - d' = 0.8h$, where h is the beam depth. Moreover, the ratio of l_b' to l_{ph} can be taken equal to 1 for low beam clear span–to–depth ratios (that is, when $l_b'/h < 5$) because plastic hinges will most likely develop in the beams at the column faces. The ratio of l_b' to l_{ph} is taken equal to 1.25 for beams with $l_b'/h \geq 5$, where gravity loading may cause the positive plastic hinges to develop away from the column face.[20] Thus, the maximum beam depth to avoid the loss of confinement action is given by substituting $(d - d')$ and (l_b'/h) in Eq. (1) for the corresponding values described and then solving for h:

$$h = \frac{\delta_{el}}{1.6\theta_f} \text{ when } \frac{l_b'}{h} < 5 \tag{2}$$

and

$$h = \frac{\delta_{el}}{2\theta_f} \text{ when } \frac{l_b'}{h} \geq 5 \tag{3}$$

Beams of reinforced concrete special moment-resisting frames detailed per ACI 318-14 can reach cord rotations of about 0.04 radians before degradation occurs.[22] This cord rotation translates into a drift ratio θ_f between 0.025 and 0.03 radians. No test data exist to assess the deformation capacity of reinforced concrete intermediate moment-resisting frames, but given the fact that the detailing of the reinforcement in the critical regions of the beams and the joints in these frames is

less stringent than that prescribed for special moment frames, the deformation capacity should be smaller. It is plausible to assume that for intermediate moment-resisting frames, θ_f ranges between 0.015 and 0.02 radians. The beam elongation δ_{el} threshold at which the confining mechanism is lost is unknown and can only be estimated through engineering judgement. In this paper, the authors assume that when δ_{el} = 13 mm (0.5 in.) there will be a loss of confinement action.

The following beam depths are calculated from Eq. (2) and (3) using the midpoint interstory drift angles within each of the two ranges and assuming δ_{el} = 13 mm (0.5 in.):

- $h < 460$ mm (18 in.) for intermediate moment frames with $l_b'/h < 5$
- $h \le 370$ mm (14.5 in.) for intermediate moment frames with $l_b'/h \ge 5$
- $h < 300$ mm (12.0 in.) for special moment frames with $l_b'/h < 5$
- $h \le 240$ mm (9.5 in.) for special moment frames with $l_b'/h \ge 5$

The beam depth limits derived for special moment-resisting frames are too small to be used in practice. Nevertheless, the beam depths calculated for intermediate moment frames are within the practical range of applications where the beam clear span between columns is less than 3.6 m (12 ft).

In summary, the untopped hollow-core diaphragms confined with reinforced concrete beams are only suitable for use with intermediate moment-resisting frames. The maximum depth of the beams derived from first principles covering all beam clear span–to–depth ratios is 370 mm (14.5 in.), a value that can be rounded up to 400 mm (16 in.).

Conclusion

Four large-scale hollow-core diaphragm specimens were tested under reversed cyclic loading. Three specimens were untopped diaphragms with variations in the boundary conditions. A fourth specimen incorporated a 50 mm (2 in.) thick cast-in-place topping slab. Tested specimens were representative of subdiaphragm regions of buildings with diaphragms of low aspect ratio where all the vertical elements are part of the lateral-force-resisting system and are tied by beams of moment-resisting frames. Variations in the boundary conditions allowed to study of the influence of the stiffness and strength of surrounding structural elements of the lateral-force-resisting system.

The cyclic performance of untopped hollow-core diaphragm specimens was highly influenced by the shear capacity along the longitudinal joints between the hollow-core slabs and the diagonal strut mechanism that developed due to the rigid body rotation of the slabs. Once the concrete shear strength along the longitudinal joints was exhausted for shear distortions of approximately 0.20%, the untopped hollow-core diaphragms were able to redistribute the internal load paths through alternative mechanisms, such as the diagonal struts, due to the rotation of the hollow-core slabs.

The early cyclic behavior of the untopped hollow-core systems appeared to be affected by the boundary conditions of the supporting beams. Although more realistic boundary conditions are difficult to represent with the test setup used, the studied rigid and more flexible boundary conditions showed a similar behavior once the diagonal strut mechanism controlled the response of the specimens.

Based on the observed and measured performances, tie connectors across transverse joints were mainly demanded by the clamping effect between the untopped hollow-core slabs and perimeter beams as these joints opened, though contribution to the resistance by a shear-friction mechanism also demanded some tensile strains on the connectors. Tension demands on these connectors due to joint opening should be considered in the design.

The cyclic behavior of topped hollow-core diaphragm specimens was influenced by the performance of the cast-in-place concrete topping because the strength of the system was limited by the fracture of the concrete topping, whereas strength degradation occurred due to the fracture of the topping reinforcement. However, nonductile performance was achieved for shear distortion demands greater than or equal to 0.75%. Untopped specimens were able to sustain the capacity for higher shear distortion demands.

The satisfactory performance of the untopped specimens may contribute to the use of this diaphragm system in buildings with the aforementioned characteristics, accounting for the geometric limitations set forth for the confining beams. Although untopped hollow-core diaphragm specimens demonstrated that they could achieve shear distortion amplitudes for shear distortion values equal to 1.5% without strength degradation, from a damage control perspective it seems reasonable to limit the shear distortion demands when designing diaphragms to avoid fractures or crushing of the corners of the hollow-core slabs.

Simplified analysis indicated the use of untopped hollow-core diaphragms confined with beams of moment frames are only suitable for buildings designed for limited ductility (intermediate moment frames) with beams of 400 mm (16 in.) deep and having an aspect ratio $l_b'/h \ge 5$.

Acknowledgments

This work was supported by the Colombian Administrative Department of Science, Technology and Innovation Colciencias and the precast concrete producer Manufacturas de Cemento SA through grant 1204-562-37641. The authors thank the anonymous reviewers for providing substantial constructive criticism.

References

1. Iverson, J. K., and N. M. Hawkins. 1994. "Performance of Precast/Prestressed Concrete Building Structures During Northridge Earthquake." *PCI Journal* 39 (2): 38–55. doi:10.15554/pcij.03011994.38.55.

2. ACI (American Concrete Institute) Committee 318. 1999. *Building Code Requirements for Structural Concrete (ACI 318-99) and Commentary (ACI 318R-99)*. Farmington Hills, MI: ACI.

3. International Code Council. 1997. *1997 Uniform Building Code*. Whittier, CA: International Conference of Building Officials.

4. NEHRP (National Earthquake Hazards Reduction Program). 1997. *Recommended Provisions for Seismic Regulations for New Buildings and Other Structures*. Washington, DC: Building Seismic Safety Council.

5. Cleland, N. M., and S. K. Ghosh. 2002. "Untopped Precast Concrete Diaphragms in High-Seismic Applications." *PCI Journal* 47 (6): 94–99. doi:10.15554/pcij.11012002.94.99.

6. Fleischman, R. B. 2014. *Seismic Design Methodology Document for Precast Concrete Diaphragms*. Vancouver, WA: Charles Pankow Foundation.

7. Schoettler, M. J. 2010. "Seismic Demands in Precast Concrete Diaphragms." Ph.D. diss., University of California, San Diego, CA.

8. Zhang, D. 2010. "Examination of Precast Concrete Diaphragms Seismic Response by Three-Dimensional Nonlinear Transient Dynamic Analyses." Ph.D. diss., University of Arizona, Tucson, AZ.

9. ASCE (American Society of Civil Engineers) and SEI (Structural Engineering Institute). 2017. *Minimum Design Loads and Associated Criteria for Buildings and Other Structures*. ASCE/SEI 7-16. Reston, VA: ASCE and SEI.

10. NEHRP. 2015. *Recommended Seismic Provisions for New Buildings and Other Structures*. Washington, DC: Federal Emergency Management Agency.

11. Hawkins, N. M., and S. K. Ghosh. 2000. "Proposed Revisions to 1997 NEHRP Recommended Provisions for Seismic Regulations for Precast Concrete Structures Part 3—Diaphragms." *PCI Journal* 45 (6): 50–59. doi:10.15554/pcij.11012000.50.59.

12. Menegotto, M., and G. Monti. 2005. "Waved Joint for Seismic-Resistant Precast Floor Diaphragms." *Journal of Structural Engineering* 31 (10): 1515-1525. doi:10.1061/(asce)0733-9445(2005)131:10(1515).

13. ACI Committee 318. 2014. *Building Code Requirements for Structural Concrete (ACI 318-14) and Commentary (ACI 318R-14)*. Farmington Hills, MI: ACI.

14. PCI Hollow Core Slab Producers Committee. 2015. *PCI Manual for the Design of Hollow Core Slabs and Walls*. MNL 126-15. Chicago, IL: PCI.

15. NIST (National Institute of Standards and Technology). 2017. *Seismic Design of Precast Concrete Diaphragms: A Guide for Practicing Engineers*. GCR 17-917-47 NEHRP Seismic Design Technical Brief 13. Gaithersburg, MD: NIST.

16. Mejia-McMaster, J. C., and R. Park. 1994. "Tests on Special Reinforcement for the End Support of Hollow-Core Slabs." *PCI Journal* 39 (5): 90–105. doi:10.15554/pcij.09011994.90.105.

17. Priestley, M. N. J. 1992. "The U.S.–PRESSS Program Progress Report." In *Third Meeting of the U.S.-Japan Joint Technical Coordinating Committee on Precast Seismic Structural Systems (JTCC-PRESSS)*. San Diego, CA: JTCC-PRESSS.

18. Angel, N. M. 2017. "Behavior of Precast Hollow Core Floor Diaphragms Subjected to Seismic Loading." Ph.D. diss., Universidad de los Andes, Bogotá, Colombia.

19. Restrepo, J. I., R. Park, and A. H. Buchanan. 1993. "Seismic Behaviour of Connections between Precast Concrete Elements." Research report 93-3, Department of Civil Engineering, University of Canterbury, Christchurch, New Zealand.

20. Fenwick, R. C., and L. M. Megget. 1993. "Elongation and Load Deflection Characteristics of Reinforced Concrete Members Containing Plastic Hinges." *Bulletin of the New Zealand National Society for Earthquake Engineering* 26 (1): 28-41.

21. Fleischman, R. B., J. I. Restrepo, S. Pampanin, J. R. Maffei, K. Seeber, and F. A. Zahn. 2014. "Damage Evaluations of Precast Concrete Structures in the 2010–2011 Canterbury Earthquake Sequence." *Earthquake Spectra* 30 (1): 277–306.

22. Visnjic, T., G. Antonellis, M. Panagiotou, and J. P. Moehle. 2016. "Large Reinforced Concrete Special Moment Frame Beams under Simulated Seismic Loading." *ACI Structural Journal* 113 (3): 469.

Notation

d = effective beam depth

d' = distance from the extreme fiber in compression to the centroid of the compression reinforcement

h = beam depth

l_b' = clear beam span

L_c = center-to-center distance between the fixed end and movable end beams

l_{ph} = distance between positive and negative beam plastic hinges within the beam span

δ_{el} = beam elongation

Δ = induced horizontal displacement measured at the middle of the cross section of the movable end beam

γ = shear distortion

θ_f = interstory drift angle

About the authors

Nelson M. Angel is a PhD student in the Department of Civil and Environmental Engineering at Universidad de los Andes in Bogotá, Colombia.

Juan F. Correal, PhD, is an associate professor in the Department of Civil and Environmental Engineering at Universidad de los Andes.

José I. Restrepo, PhD, is a professor in the Department of Structural Engineering at the University of California–San Diego.

Abstract

This paper highlights the results of the experimental phase of a comprehensive research project on the seismic performance of hollow-core diaphragms. The four specimens tested resembled a subdiaphragm region framed by beams. Variations in the boundary conditions of the hollow-core slabs and the inclusion of a cast-in-place concrete topping slab were considered. A bidirectional test fixture was used for simultaneous control of in-plane lateral load and bending deformations. Global and local behaviors were examined under a sequence of increasing cyclic demands. Untopped hollow-core diaphragm specimens exhibited stable behavior that was influenced by shear strength along longitudinal joints and a bearing mechanism that developed between the hollow-core slabs and the supporting beams. The performance of the topped specimen was affected by localized damage to the cast-in-place concrete topping and large demands on the welded-wire mesh reinforcement.

Keywords

Diaphragm, experimental performance, hollow-core slab, topped diaphragms, untopped diaphragms.

Review policy

This paper was reviewed in accordance with the Precast/Prestressed Concrete Institute's peer-review process.

Reader comments

Please address any reader comments to *PCI Journal* editor-in-chief Emily Lorenz at elorenz@pci.org or Precast/Prestressed Concrete Institute, c/o *PCI Journal*, 200 W. Adams St., Suite 2100, Chicago, IL 60606.